



## Iraqi Journal of Applied Physics



P. O. Box 88052, Baghdad 12001, IRAQ

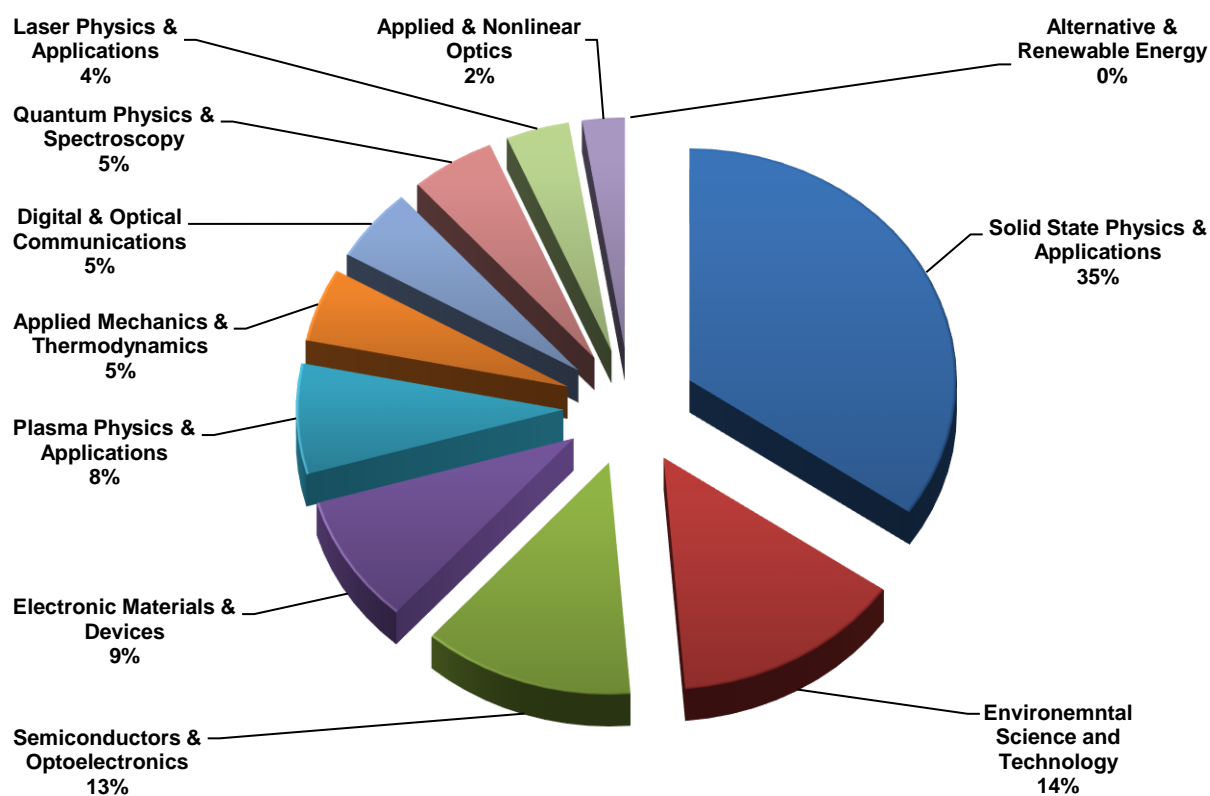
[www.iraqiphysicsjournal.com](http://www.iraqiphysicsjournal.com)

Email: [info@iraqiphysicsjournal.com](mailto:info@iraqiphysicsjournal.com)

Email: [editor\\_ijap@yahoo.co.uk](mailto:editor_ijap@yahoo.co.uk)

Email: [irq\\_appl\\_phys@yahoo.com](mailto:irq_appl_phys@yahoo.com)

Email: [ijap.editor@gmail.com](mailto:ijap.editor@gmail.com)



# Subject Index 2005-2023

## Alternative & Renewable Energy

IJAP-AARE

- General Characteristics of High Energetic Proton Events Observed with SOHO/ERNE During Solar Cycle 23, 10(4), 3
- Nuclear Green Energy, 10(1), 3
- Characterization of Laser-Ablated Nanostructured  $\text{Al}_2\text{O}_3/\text{p}$ -Solar Cells, 11(1), 29

## Applied & Nonlinear Optics

IJAP-AANO

- Analytical Study on Effect of Lateral Shear Interferogram on Path Difference in Coherent Optical Systems, 18(2), 11
- Computer Aided Design of a Magnetic Lens Using a Combined Dynamic Programming and Artificial Intelligence Technique, 10(1), 33
- Control of Nonlinear Dynamics in Semiconductor Laser with Optoelectronic Feedback, 15(1), 3
- Curvelet-Based Optical Flow Estimation Algorithm Based on Central Derivatives, 6(2), 13
- Design of a Multi-Electrode Immersion Lens for Ion-Optical Systems, 2(1,2), 27
- Design of All-Reflecting Aplanatic Objective, 9(3), 19
- Development of an Inverted Optical Tweezers with Full Motional Control, 7(2), 19
- Investigations of Linear and Nonlinear Optical Properties of Transparent ZnO Thin Films Grown by Sol-Gel Method, 6(3), 29
- Key Mechanisms of the Nonlinear Amplification: Physics and Applications, 1(2), 3
- Microscopic Imaging of Red Cell Aggregation with Photoacoustic Technique, 18(4), 3
- Microstructural Features and Properties of High-Hardness and Heat-Resistant Dispersion Strengthened Copper by Reaction Milling, 8(4), 3
- New Method for Calculating Cumulative Line Energy Using Pupil Function Technique, 2(1,2), 7
- Numerical Analysis of Temperature Dependencies of Optical Elasticity Coefficient on Lens Induced in Solid-State Laser Crystal, 14(2), 35
- Some Optical Properties of an Electrostatic Immersion Lens Using the Charge Density Method, 1(4), 21
- Tapering and Metallizing Optical Fibers by Immersion in Buffered Aqueous Solution with Different Molar Ratios, 18(2), 33
- Temperature-Dependent Birefringence Properties of  $\text{Be}_3\text{Al}_2\text{Si}_6\text{O}_{18}$  Crystal, L2(1), 12

- Thermogravimetric Properties of Porcelain Supported by Addition of Beryllium Oxide, 17(3), 27
- Fine Control of Refractive Index in Large-Size Magnetic Fluids for Photonics Applications 19(4B), 127
- Refractive index fine control in large size samples of magnetic fluids for photonic Applications 19(4C), 257

## Applied Mechanics & Thermodynamics

IJAP-AMAT

- Analytical and Experimental Study on Bound and Free Surface Waves in Wind-Wave Tank System, 8(1), 11
- Analytical Calculation of Heat Conduction in Two-Phase Heterogeneous Materials, 7(4), 11
- Characterization of D.C. Sputtering System, L1(1), 3
- Employing Inner Triplet Upgrade in Cold Mass Cooling Design for Large Hadron Collider, L2(1), 19
- Ferrohydrodynamic Instability of a Couple Stress Magnetic Fluid Layer Under the Influence of Time-Dependent Sinusoidal Magnetic Field, 18(4), 15
- HAZ Extent Analysis in Fiber-Reinforced Plastic Grooving by Laser, 1(1), 3
- Investigation of Bound and Free Surface Waves in Microwave and Acoustic Wind-Wave Tank Systems, 14(2), 11
- Optimization of Composition, Structure and Characteristics of Metal in Arc Deposition, 5(2), 37
- Marangoni Convection Effect on the Melting of GaSb/InSb/GaSb Sandwich Structured Sample, 4(2), 35
- Modeling of the Preheating Effect on Keyhole Laser Welding Efficiency, L1(1), 10
- Performance of Thermally Regenerative Electrochemical Cycles System, 18(2), 3
- Structural, Electronic and Thermal Properties of TiC Compound in Sodium Chloride Structure, 11(1), 9
- Torque and Magnetic Flux Analysis Using an Advanced Dynamic Dynamometer Test Bed for Electromechanical Motors, 5(1), 13
- Using Longitudinal Surface Acoustic Waves for Non-Destructive Testing of Inner Surfaces, L1(2), 9
- Adsorption, Kinetics, Thermodynamics, and Isothermal Studies of Phenol Red Dye Adsorption Using Activated Charcoal Prepared from Khestawi Dates 19(4B), 93
- Effect of Polyimide Layer on Surface Dielectric Barrier Discharge Characteristics Studied for the Air Flow Improvement 19(4B), 103

- Thermoelectric Performance of Metallophthalocyanine Molecular Junctions with CIP and CPP Configurations 19(4B), 133

### Digital & Optical Communications

IJAP-DAOC

- A Balanced Backoff Algorithm for IEEE802.11 Wireless Network, 8(1), 27
- A CPW-Fed Printed Monopole Ultra-Wideband Antenna with E-Shaped Notched Band Slot, 6(4), 17
- A New Fractal Microstrip Bandpass Filter Design Based on Dual-Mode Square Ring Resonator for Wireless Communication Systems, 5(1), 7
- A Novel Secure Digital Watermark Generation from Public Share by Using Visual Cryptography and MAC Techniques, 10(3), 3
- Analysis and Design of Combined Fractal Dipole Wire Antenna, 5(2), 29
- Application of Multiple Coded Frame Temporal Processing to Enhance Digital Image Transfer for High-Definition Communications Systems, 14(1), 27
- Classification of Digital Modulation Using Wavelet Transform, 1(3), 15
- Coherent Detection in Optical Fiber Systems, 3(1), 3
- Comparative Evaluation of Bit Error Rate in Frequency Selective Fading Channels Employed in Wavelet Modulation, L1(2), 14
- Crosstalk and Noise in Optical Amplifier with Gain Clamping by Vertical Laser Field, 16(2), 17
- Design and Analysis of Special Small Size Cross Dipole Antenna, 6(2), 19
- Design and Implementation of Adaptive Antenna System in a New LTE 3GPP Transceivers Based Multiwavelet Signals, 10(2), 11
- Design and Implementation of Adaptive Antenna System in Physical Layer CDMA Transceivers Based Multiwavelet Signals, 11(1), 3
- Design of Low-Cost Multi-Waveforms Signal Generator Using Operational Amplifier, 14(1), 13
- Determination of The Satellite Images Orientation Using DCT Coefficients, 6(2), 31
- Dipole Antenna with Fractal Koch Curve Geometry for Multiple Frequency Applications, 7(2), 3
- Effect of Chirping on Received Pulse Shape in Optical Fiber Communications, L2(2), 7
- Frequency-Selective Surface for Reduced Mutual Coupling among Closely Spaced Array Antenna, 14(1), 19
- FSK Transceiver for Bit Error Rate Tester Implementation, 8(4), 9
- Influence of Magnetic Saturation on Sensorless Rotor Position Estimation in IPMSM Drives Based on HIL Simulator, 8(3), 3
- Linear Adaptive Antenna Array Geometry Effects on Radiation Pattern, L3(1), 3

- New Algorithm for High Throughput of IEEE 802.11 Distributed Coordination Function, 14(2), 27
- Novel Optical Fiber Sensor Based on SGMS Fiber Structure for Measuring Refractive Index of Liquids and Gases, 7(4), 17
- Probabilistic Roadmap, A\*, and GA for Proposed Decoupled Multi-Robot Path Planning, 10(2), 3
- Performance Optimizing of Fourth Order Delta-Sigma Fractional-N Frequency Synthesizer using a Dither Technique for Third Generation (3G) Applications, 7(1), 3
- Phase Noise Compensation for Coherent Orthogonal Frequency Division Multiplexing in Optical Fiber Communications Systems, 5(2), 3
- Quantum Limit Characterization of Signal-to-Noise Ratio using Phase-Shift Keying in Homodyne Detection, L3(1), 11
- Range-Coverage Extension Using Smart Antennas in Mobile Communications Systems, 5(2), 25
- Reliable Implementation of Paillier Cryptosystem, 10(4), 27
- Signal Mechanism Analysis of Fiber Arrival Time in Fiber Optic Pin, 5(2), 13
- Software Defined Radio (SDR) Methodology Based Multi-Core Software Platform, 9(4), 3
- Synchronization Scheme for Secured Communications System Based on Chaotic Signals, L3(1), 7
- Transmission of Compressed Video Signals through Spread Spectrum Channel, 6(4), 9
- A Method to Improve the Security Level of Advanced Encryption Standard Algorithm by Using Proposed Algorithm, 8(4), 29
- Bandwidth Enhancement for Annular Dielectric Resonator Antenna (ADRA) Using Stacked Technique 19(4A), 37
- Bandwidth Enhancement of Cylindrical Circular Microstrip Antenna Using Slots Technique 19(4A), 55
- Chaotic Semiconductor Laser with Extra Optical Delay Feedback 19(3A), 31
- Design and Simulation of Rectangular Microstrip Patch Antenna Using a Computer Simulation Technology Operating at 4.5 GHz 19(2), 53

### Electronic Materials & Devices

IJAP-EMAD

- Analysis of Atomic and Electronic Structures of NiO/Au Interfaces by High-Resolution MEIS and Photoelectron Spectroscopy, 14(3), 13
- Characteristics of Cu<sub>2</sub>O-Doped Sn<sub>2</sub>O<sub>3</sub> Nanostructures Deposited on Porous Silicon Substrates as Gas Sensors, 18(1), 27
- Characteristics of Multilayer glass/ITO/N:TiO<sub>2</sub>/NiO/KOH/Pt/glass Photoelectrochromic Device Synthesized by Reactive Magnetron Sputtering, 18(3), 11

- Characterization of CdSe/Si Heterostructures Synthesized by Plasma-Induced Bonding Technique, 18(1), 21
- Characterization of E-Mode InZnO Thin Film Transistors Produced by DC Sputtering Technique, L3(1), 19
- Comparison of Electro-optical Effects in Pure and Cobalt Nanoparticles-Doped 6CHBT Liquid Crystals, 15(1), 5
- Dark and Illumination Electrical Characteristics of ZnS/Si Heterojunction Prepared by Pulsed Laser Deposition, 11(2), 25
- Determination of Electronic Properties of Gallium Nitride Structure Using Density Functional Theory, 17(4), 19
- Development of NVD's Using XR5<sup>TM</sup> IIT Technique and III-V Photocathode Under Night Sky Conditions, 7(4), 33
- Effect of Heat Treatment on the Optical Properties of ZnO Thin Films Prepared by Chemical Spray Method, 9(1), 23
- Effect of Substrate Temperature on Structural Characteristics of Nano Silver Oxide Prepared by Pulsed-Laser Deposition, 11(2) 33
- Electrical Properties of Cu<sub>2</sub>O Films Prepared by Electro-Deposition Method, L1(2), 27
- Empirical and Simulation of Thermal Insulator of SWCNTs – Ceramic/Polymer Nanocomposites, 7(4), 3
- Enhancement of Current Gain at High Collector Current Densities for Silicon-Germanium Heterojunction Bipolar Transistors, 16(1), 9
- Extraction of Doping Profile in Substrate of MNOS capacitor Using Fast Voltage Ramp Deep Depletion C-V method, 6(1), 35
- Fabrication and Characterization of InZnO TFTs Grown on Transparent Conductive Oxide Substrate by DC Sputtering Technique, 6(1), 41
- Fabrication and Characterization of Silver-Doped Nickel Oxide Thin Films for Gas Sensors, 18(3), 3
- Field Dependent Critical Trap Density for Thin Gate Oxide Breakdown, 6(3), 15
- Fundamentals of Microwave Integrated Circuits Based on High-Temperature Superconductors, 9(3), 3
- Incorporation of Gold Nanoparticles in Single-Atomic Layered Materials and Their Plasmonic Absorption Characteristics as Highly-Efficient Nonlinear Optical Media, 17(1), 33
- Junction Characteristics of Wide-Emitter (p)CdS-(n)Si-(p)Si Heterojunction Transistor, 2(1,2), 3
- Nanostructure Dopants TiO<sub>2</sub> Films for Gas Sensing, 7(2), 27
- New High Angular Resolution Detection System for Direction Recognition, 1(3), 27
- Optimized Characteristics of Silver Nanoparticles Synthesized by Chemical Reduction and Embedded in Silica Xerogels, 18(3), 25
- Performance Comparison of InP-Based Phototransistors to PIN and UTC Photodiodes, 4(4), 13
- Recent Developments in Silicon Photomultipliers, 4(3), 27
- Resistance-Time Characteristics of MEH-PPV/Si Device for Gas Sensing Applications, 17(3), 21
- Structural and Gas Sensing Characteristics of CuO-Doped ZnO Thin Films Papered by Pulsed-Laser Deposition, 15(4), 3
- Structural and Optical Characteristics of Co<sub>3</sub>O<sub>4</sub> Nanostructures Prepared by DC Reactive Magnetron Sputtering, 18(4), 31
- Study on Compensation of Thermal Stresses in the Fabrication Process of Thin-Film Transistor, L1(1), 28
- Synthesis and Characteristics of Electrochromic Glass with Multi-Layer Configuration Based on glass/ITO/WO<sub>3</sub>/ZrO<sub>2</sub>/NiO/ITO/glass, 15(4), 17
- Synthesis of Antimony Oxide Nanoparticles by Pulsed Laser Ablation in Wet Media, 9(3), 13
- Wide Range Speed Control Based on Field Oriented Control of Permanent Magnet Synchronous Motor, 9(4), 21
- Wideband (0.6-11) micron Angle Deposited Thin Te:S Laser Detector, 1(4), 3
- Underwater Sensing Characteristics of a ZnO Thin Film Sensor Prepared by Spray Pyrolysis, L1(1), 24
- Characterization of Nickel-doped PVA Gas Sensors Fabricated by Electrospinning Method 19(4B), 163
- Characterization of ZnO-SnO<sub>2</sub> Nanostructures Prepared by Thermal Evaporation Technique as Gas Sensor 19(4C), 243
- Effect of Copper Dopants on Structural and Optical Properties of Nickel Oxide Thin Films as NO<sub>2</sub> Gas Sensors 19(4C), 187
- Effect of In<sub>2</sub>O<sub>3</sub> and Eu<sub>2</sub>O<sub>3</sub> Dopants on Morphology and Gas Sensing Properties of CeO<sub>2</sub> Thin Films 19(3A), 11
- Highly-Sensitive Room-Temperature Ammonia Gas Sensor Fabricated from Modified Copper Oxide Nanostructures 19(4C), 197
- Investigation of Electrical, Optical Properties and Thermal Sensitivity of MEH-PPV/Ag Thin Films 19(4C), 175
- Investigation of Sensitivity of Silver-doped Tin Oxide Nanostructures to Nitrogen Dioxide Gas 19(4B), 121

## Environment Science & Technology

IJAP-ENST

- Determination of Uranium and Thorium levels and Measurement of Annual Effective Dose levels in Some Canned Foods, 18(3), 31
- Using Banana Peels for Green Synthesis of Mixed-Phase Titanium Dioxide Nanopowders, 18(4), 21
- Effect of Laser Power on Optical Properties of CN-85 Nuclear Track Detector 19(3B), 39



- Green Synthesis and Characterization of Silver Nanoparticles for Biological Applications 19(3A), 59
- Indoor Radon Measurements in Some Nineveh Plain Region Homes Using a Small Container with CR-39 Detector 19(3B), 9
- Isolation of Fungi from Petroleum-Contaminated Soil and Evaluation of Their Ability to Degrade Crude Oil 19(1) 13
- Measurement of Uranium and Radon Concentrations in Wells Water Samples of Some Farms near the Mosul City in Iraq 19(3B), 3
- Nano Nigella Sativa Used as Free Radicals Scavenger 19(4B), 171
- Nonlinear Control Back Stepping Controllers for Max Power Point Tracking in Photovoltaic Systems under Variable Environmental Situations 19(4B), 139
- Physical Properties of Biogas Produced by Anaerobic Treatment of Household Waste in Samarra City for Thermal Energy Production 19(2), 38
- Radium and Uranium Concentrations in Some Fruits and Vegetables Cultivated in Nineveh Governorate, Iraq 19(3B), 15
- Synthesis of Activated Carbon Nanoparticles from Date Seeds to Remove Malachite Green 19(4A), 13
- Synthesis of Copper Nanoparticles Using Liquorice Extract as Reduction Agent and Their Antibacterial Properties 19(4C), 191
- Effect of Self-Absorption on the Output Power of CW CO<sub>2</sub> Laser, L2(1), 31
- Effects of Semiconductor Laser Bias Current on Synchronization in Chaotic Dynamics, 15(4), 11
- Effect of Transverse Magnetic Field on Laser Beam Width Parameter, 8(3), 31
- Fabrication of Solid Random Gain Media in Visible Region from Rhodamine Dye Solutions Containing Highly-Pure Titanium Dioxide Nanoparticles, 18(1), 3
- Femtosecond Ti:sapphire Laser Pulses to Deposit Precious Metal Nanoparticles on Crystalline and Amorphous Titanium Dioxide Films, 14(2), 43
- Gaussian to Super-Gaussian Laser Beam Intensity Profile Conversion using Glass Micro-Optic Fabricated with Reflowed Photoresist, 16(2), 3
- HAZ and Melt Limits of 3-D CO<sub>2</sub> Laser Welding, 7(2), 11
- Improvement of Wound Healing in Rabbit Skin by Low Level Polarized Laser Light, 9(4), 29
- Laser-Assisted CVD Fabrication and Characterization of Carbon and Tungsten Microhelices for Microthrusters, 3(3), 3
- Laser-Controlled Photoluminescence Characteristics of Silicon Nanocrystallites Produced by Laser-Induced Etching, 1(1), 15
- Laser-Human Skin Interaction: Analytical Study and Optimization of Present Non-Ablative Laser Resurfacing, 4(3), 5
- Modeling of 3-D Keyhole CO<sub>2</sub> Laser Welding of Steel, 6(1), 15
- Modeling of Plume Dynamics in Laser Ablation with Application to Nanotubes Synthesis, 16(2), 25
- Modeling of Temperature-Dependent Absorptivity of Laser-Treated Surface, 6(3), 21
- Non-ablative Tattoo Removal Using Fundamental and Second Harmonic Nd:YAG Laser (Histological Observations), 9(4), 11
- Non-Ablative Tattoo Removal Using Fundamental and Second Harmonic Nd:YAG Laser (Tattoo Ink Clearance Response), 10(1), 21
- Optical Properties of Silicon Nanoparticles Produced by Nd:YAG Laser Ablation, 4(4), 19
- Performance Optimization of Multi-Quantum Wells Laser Used in Optical Communications, L2(2), 11
- Profiling of Antimony Diffusivity in Silicon Substrates using Laser-Induced Diffusion Technique, L3(1), 23
- Simultaneous Amplitude-Modulation and Harmonic Frequency-Modulation Mode Locking of Nd:YAG Laser, 16(2), 11
- Structural Characteristics Study of Indium Diffusion in Silicon Using a Pulsed Nd:YAG Laser, 1(1), 34
- Studying of Reflected Light Optical Laser Microscope Images Using Image Processing Algorithm, 9(1), 15
- Temperature Dependencies of Refractive Index and Optical Elasticity Coefficient on Lens Induced in Nd:YAG Crystal, 8(1), 35

### Laser Physics & Applications

IJAP-LPAA

- (3-5) $\mu$ m and (8-12) $\mu$ m Wavelengths Ultra-Short Tunable Laser Pulses Using Optical Parametric Oscillation Technique, 4(4), 37
- A Line Tuned TM<sub>00</sub> Mode CW CO<sub>2</sub> Laser, 1(1), 8
- Accurate Relative Frequency Cancellation Between Two Independent Lasers, 2(3,4), 3
- Characterization of Diode Laser-Pumped Nd:YVO<sub>4</sub> Disk Laser, 4(2), 31
- Characterization of Quantum Well Diode Pumped Nd:YVO<sub>4</sub> Using V-Shape Technique, L1(1), 31
- Continuous-Wave Broadly Tunable Cr<sup>2+</sup>:ZnSe Laser, 2(3,4), 6
- Design and Simulation of DPSS Laser with SHG for Material Processing, L2(1), 3
- Design and Simulation of Q-Switching and Mode-locking Nonlinear Mirror for Frequency-Doubled DPSS Nd:YAG Laser Output, 7(4), 23
- Design, Construction and Operation of a Multi-Stage Large-Bore CO<sub>2</sub> Laser, 1(1), 25
- Development of UV Raman LIDAR System to Measure Temperature and Water Vapour Profiles in Troposphere Layer, 14(2), 19
- Effect of Active Medium Temperature on the Output Characteristics of Pulsed Free-Running R6G and RB Dye Laser, 1(1), 30

- Terahertz Lasing Using Optically Excited Neutral Donor Centres Embedded in Crystalline Silicon, 16(3), 21
- Using Frequency Resolved Optical Gating for Optimization of Thermal Lensing Compensated Ti:Sapphire Femtosecond Laser System, 11(3), 9
- Effect of Laser Frequency on Nonlinear Optical Properties of ZnO Thin Films 19(3B), 25
- Influence of Light Intensity and Irradiation Time on Efficacy of Polymerization Temperature Using Diode Laser and Light-Emitting Diodes 19(3B), 35
- Physical Characterization and Antibacterial Activity Evaluation of Nanoparticles Manufactured from Zinc Plate by Pulsed Laser Ablation 19(2), 3

### Plasma Physics & Applications

#### IJAP-PPAA

- Advanced Laser Diagnostics for Non-Equilibrium Plasma Assisted Combustion Kinetics, 14(2), 3
- Analysis of Boltzmann Equation for SF<sub>6</sub> and Some Gas-Mixture Discharges at Critical Field Condition, 12(1), 31
- Analysis of Secondary Electron Emission in Gas Glow Discharges Used for Thin Film Deposition Processes, 16(1), 15
- Breakdown and Langmuir Electrical Characteristics of Glow Discharge Plasma in DC Reactive Dual-Magnetron Sputtering System, 16(1), 3
- Characterization of Low-Pressure Argon and Nitrogen Discharge Plasmas Using Electrical Floating Probe Method, 9(3), 25
- Current-Voltage Characteristics of DC Plasma Discharges Employed in Sputtering Techniques, 12(3), 10
- Determination of Electron Temperatures in Rare-Gases Plasma, 4(1), 5
- Effect of Adding Nitrogen to the Gas Mixture on Plasma Characteristics of a Closed-Field Unbalanced DC Magnetron Sputtering System, 10(1), 27
- Effect of Annealing on the Electrical Characteristics of CdO-Si Heterostructure Produced by Plasma-Induced Bonding Technique, 4(3), 33
- Effects of Dual-Magnetron Configuration on Electrical Characteristics of Argon Discharge Plasma, 18(3), 17
- Employment of Magnetron to Enhance Langmuir Probe Characteristics of Argon Glow Discharge Plasma in Sputtering System, 12(4), 19
- Generation of Highly-Directed Laser-Driven Plasma Blocks for Light Ion Beam Fusion Applications, 6(1), 3
- Influence of Inter-Electrode Distance, Gas Mixing, Magnetic Field and Cathode Material on Breakdown Voltage of Lab-Made DC Magnetron Sputtering Device, 10(4), 21

- Influence of Magnetic Nitrogen Plasma Functionalization of High Density Polycarbonate, 8(4), 17
- Isentropic and Isenthalpic Cooling Techniques for Low-Temperature Discharges, 15(4), 29
- Langmuir Probe Diagnostics of Low-Pressure Glow Discharge Plasma Using Argon-Nitrogen Mixtures, 12(2), 17
- Laser-Based Measurements in Non-Equilibrium Plasmas, 8(1), 3
- Magnetic Field Distribution of Closed-Field Unbalanced Dual Magnetrons Employed in Plasma Sputtering Systems, 12(3), 35
- Microhardness and Tension Measurements of Pulsed-Laser Surface-Treated Aluminum Alloys, 11(3), 21
- Monte Carlo Simulation of Electronic Kinetics in Gas Discharge, 1(3), 3
- Numerical Model to Estimate the Potential Changes within Laser-Solid Surface Interaction Zone, 6(2), 3
- One-Dimension Simulation of Plasma Flow in the Cylindrical Hall Thruster, 8(4), 23
- The Fundamentals of Plasma-Assisted CVD Technique Employed in Thin Films Production, 11(2), 3
- Design and Development of Atmospheric Pressure DBD Ar Plasma Jet for Investigating Cotton Fabric Hydrophilicity 19(4C), 205
- Effect of Plasma Exposure Time on Structural Characteristics of Copper Acetyl-acetonite Films Prepared by Thermal Evaporation 19(2), 21
- Effective Treatment Method for Skin Wounds Using Cold Plasma 19(2), 56
- Effects of Magnetic Field on Growth and Electrical Characteristics of Tornado Gliding Arc Discharge 19(4C), 235
- Optical Quality of Copper Oxide Nanoparticles Prepared by Plasma Jet Electrolysis Technique 19(2), 48
- Plasma Evolution within Streamer Discharge Channels at Transition between 2nd and 3rd Mode of Discharge 19(3A), 3

### Quantum Physics & Spectroscopy

#### IJAP-QPAS

- Alternative mechanisms for electroweak symmetry breaking, 8(2), 8
- Application of Hydrotropic Solubilization Phenomenon for Estimating Diacerein in Capsule Dosage Form by Spectrophotometry Methods, 8(3), 17
- Beating Classical and Quantum Limits in Optics, 3(2), 3
- Calculation of Charge Density Distribution of (2s-1d) Shell-Model Nuclei Using the Occupation Numbers of States, 2(1,2), 31
- CERN experiments observe particle consistent with long-sought Higgs boson, 8(3), 11

- Characterization of Highly-Pure Silicon Dioxide Nanoparticles as Scattering Centers for Random Gain Media, 16(2), 37
- Correction Four-Component Dirac-Coulomb Using Gaussian Basis-Set and Gaussian Model Distribution for Super Heavy Element ( $Z=115$ ), 12(1), 17
- Design of a Fundamental Concept of Virtual Reality System for Intensity Distribution in Free Electron Laser Amplifier, 4(1), 11
- Dispersion Compensation for a Femtosecond Self-Pumped Phase Conjugator, 2(3,4), 9
- Effect of Acidic Environment on the Spectral Properties of *Hibiscus sabdariffa* Organic Dye used in Dye-Sensitized Solar Cells, 10(2), 27
- Effect of Dissipative Forces on the Theory of a Single-Atom Microlaser, 2(3,4), 12
- Effect of Oxygen Quencher on Absorption and Fluorescence Spectra of Rhodamine-6G and Rhodamine-B Dyes in Ethanol Solvent, 1(1), 20
- Effect of the Scattered Solar Radiation on the Atmospheric Ozone Measurements, 2(1,2), 11
- Effect of Thermal Annealing on Photoluminescence Characteristics of Titanium Dioxide Thin Films Doped with Copper Oxide by Pulsed-Laser Deposition, 17(4), 15
- Effective Collection and Transformation of Emission into Directional Radiation Based on Surface Plasmon-Coupled Emission, 17(1), 21
- Effects of Rare Earth Dopants on Spectroscopic Properties of Silica Glasses Prepared by Sol-Gel Technique, 16(3), 3
- Effects of Solvent Properties on Absorption and Fluorescence Characteristics of Two Organic Dyes Used as Random Gain Media, 17(2), 15
- Effects of Temperature and Concentration on Spectroscopic Behaviors of Laser Dye, 12(1), 35
- Elusive particle may be near, 8(2), 26
- Energy Transfer Calculations Based on Fluorescence Spectra of Acriflavine and Rhodamine B Laser Dyes, 16(3), 33
- Experimental Observations and Modelling of Electron Density of the Plasmasphere, 6(1), 47
- Extra Val Function for the Theoretical Sensing of Ultraviolet Light and Temperature Produced by Fluorescein-Filled Photonic Crystal Fiber, 13(3), 29
- Fluorescence Characteristics of Coated-Cell Dye Solutions Containing Highly-Pure Nanoparticles as Random Gain Media, 18(1), 35
- Fluorescence Characteristics of Highly-Pure Nanoparticles Embedded in Dye Complexes for Random Laser Design, 18(2), 27
- Fluorescence Energy Transfer Characteristics in Binary Acriflavine-Red Nut Lasing Dye Mixtures, 12(2), 3
- Fractal Nanotechnology, 4(4), 25
- FTIR Spectra of Molybdenum Tellurite Glasses, 2(1,2), 23
- FTIR Spectroscopic and Computational Studies on Hydrogen Adsorption on the Zeolite Li-FER, 4(2), 21
- General Characteristics of High Energetic Proton Events Observed with SOHO/ERNE During Solar Cycle 23, 10(4), 3
- Generation of Femtosecond Pulses from Order-of-Magnitude Pulse Compression in a Synchronously Pumped Optical Parametric Oscillator Based on Periodically Poled Lithium Niobate, 2(3,4), 24
- Generation of Intense 8-fs Pulses at 400nm, 2(3,4), 15
- Higgs Boson, 8(2), 3
- High-Intensity Third-Harmonic Generation in Beta Barium Borate Through Second-Order and Third-Order Susceptibilities, 2(3,4), 18
- Introduction to the Higgs Boson Papers, 8(2), 12
- Introduction to Particle Physics and the LHC, 8(2), 23
- Luminescence Characterization of the Bio-Conjugated Quantum Dots with CA125 Antigen Using Linkage Molecules, 7(1), 27
- Luminescent Plates Doped with Stilbene 420 Dye for Enhanced Silicon Solar Cell Performance: Down-Conversion, 6(4), 3
- Measurements of *d*-band Center Shifts of Titanium Dioxide Catalyst Using Gold Nanoparticles in Carbon Monoxide Oxidation Reaction, 14(3), 3
- Measurement of Water Vapour and Temperature Profiles Within the Troposphere Using Ultraviolet Raman LIDAR System, 8(1), 19
- Medium Energy Ion Scattering Spectrometry of Helium Ions Scattered from Rutile Titanium Dioxide Surfaces, 14(3), 29
- Nanolasers: Lasing from Nanoscale Quantum Wires, 3(4), 3
- Near-Edge X-ray Absorption Fine Structure Analysis of Magnesium-Palladium Nanoparticles Fabricated by Gas Evaporation Method, 14(3), 35
- Optical Emission Spectroscopy of Laser-Produced Plasmas of Some Metal Targets, 18(1), 15
- Optimization and Fine-Tuning of Controlled White-Light Continuum Generation in Transparent Solid Medium by 1-kHz Repetition Rate Femtosecond Laser Pulses, 12(1), 27
- Phase Conjugation with Random Fields and with Deterministic and Random Scatterers, 2(3,4), 21
- Preparation and Characterization of Dysprosium-Doped Titanium Dioxide Photocatalyst by Sol-Gel Method, 17(3), 3
- Silicon Dioxide Nanostructures-Coated External Cavity for Gain Enhancement of Rhodamine B Lasing Dye, 14(1), 3
- Some Physical Properties of Metal-Hydroxyquinoline Complexes in Different Solvents, 17(1), 9
- Spectroscopic Study of Chromium-Doped Silicon Nitride Nanostructures Prepared by DC Reactive Magnetron Sputtering, 17(2), 11

- Spectroscopic Study of Sol-gel Synthesized Silica Xerogel Embedded with Dysprosium Ions, 18(4), 3
- Synchronization in Optically Coupled Chaotic Systems by Optical Feedback, 12(1), 11
- Synchrotron-Radiation Infrared Microscopy Analysis of an Amyloid Peptide Irradiated by Mid-Infrared Free-Electron Laser, 14(3), 41
- The biggest machine in the world, 8(2), 22
- The Mythical Higgs Boson, 8(2), 26
- Finding the Smallest Unifying Particle in the Human Universe: An Artistic Theory of Everything, 8(2), 27
- X-Ray Absorption Fine Structure Spectroscopy of Alumina-Supported Copper Oxide for Conversion Electron Yield Detection, 14(4), 29
- Calculations of Nuclear Two-Component State Density in Non-Equidistant Spacing Model with Modified Williams' Formula 19(2), 15
- Spectral analysis and enhancement of  $\text{Sm}^{3+}$  photoluminescence in sol-gel derived  $\text{Sm}^{3+}$ -Ag<sup>+</sup> co-doped silica xerogels 19(4A), 29
- Spectroscopic Characteristics of Silicon Nitride Thin Films Prepared by DC Reactive Sputtering Using Silicon targets with Different Types of Conductivity 19(4A), 73
- Study of Thermal Effect on Physical Properties of PEG8000/TiO<sub>2</sub> Composite Using Positron Annihilation Lifetime Spectroscopy 19(2), 27

### Semiconductors & Optoelectronics

IJAP-SCAOE

- Analysis and Simulation of Carrier Transport in InP-Based Double Heterojunction Photoelectronic Device, 13(3), 23
- Annealing Effect on the Photoluminescence of CdTe/CdSe Thin Film Photovoltaic Devices, 1(3), 23
- Band Diagram of p-PbTe/n-Si Heterostructure, 1(2), 27
- Characteristics of a-Si:H Solar Cell Under Extended Illumination Condition Using NIR Laser, 5(1), 35
- Characteristics of p-n Junction Silicon Carbide LED, 2(1,2), 17
- Characterization of  $(\text{CdO})_{1-x}(\text{ZnO})_x$  Thin Films Prepared by Pulsed-Laser Deposition for Solar Cell Applications, 11(3), 3
- Characterization of CdS:In/Si Heterojunction Solar Cells, 1(2), 13
- Characterization of SiC/Si Heterojunction Fabricated by Plasma-Induced Growth of Nanostructured Silicon Carbide Layer on Silicon Surface, 12(2), 9
- Charge Injection into Organic Semiconductors, 4(2), 5
- Computation of Optical Energy Gap of Cu<sub>2</sub>O Thin Film: Theoretical Estimation, L1(1), 21
- Correlation Between Kinematics, Optical and Structural Properties of Size Quantized PbS Nano Films Deposited by Spray Pyrolysis, 10(3), 35
- DC Conductivity and Optical Properties of InSbTe<sub>3</sub> Amorphous Thin Films, 6(3), 9
- Density of Defect States in  $\text{Se}_{90}\text{Sb}_{10-x}\text{Ag}_x$  Glassy Alloys, 9(4), 25
- Determination of Energy Band Outline of CoO:Au/Si Thin Film Solar Cells, 17(3), 17
- Effect of Annealing Temperature on Urbach Energy for CdO:In<sub>2</sub>O<sub>3</sub> Thin Films Prepared by Pulsed-Laser Deposition, 16(1), 21
- Effect of Bath Temperature on the Optoelectronic Characteristics of Chemically Deposited CdS Thin Films, 5(1), 23
- Effect of pH Value on the Photoconductivity of Chemically Deposited CdS Thin Films, L2(1), 23
- Effect of Thickness on Optical and Electrical Properties of ZnO Prepared by CBD, 7(1), 11
- Effect of Using Organic Stabilizing Agent on Structural Characteristics of Cadmium Telluride Quantum Dots, 17(3), 13
- Effects of Deposition Parameters on Chemically Deposited PbS Thin Films, 4(4), 7
- Effects of Temperature on The Properties of Amorphous-to-Crystalline Transition in AgSbSe<sub>2</sub> Thin Films, 7(1), 17
- Efficiency Enhancement of Photovoltaic Silicon Cell by Ultrashort Laser Pulses, 5(2), 33
- First Principle Calculation of Pressure-Induced Phase Transition and Band Structure of Gallium Phosphide, 9(4), 17
- Gas Phase Growth Techniques for Quantum Dots: An Overview, 14(4), 3
- Growth of  $\text{In}_x\text{Ga}_{1-x}\text{Sb}$  Bulk Crystals by Czochralski Technique, 1(4), 17
- Heterojunction Solar Cell Based on Highly-Pure Nanopowders Prepared by DC Reactive Magnetron Sputtering, 16(3), 27
- High-Quality Plasma-Induced Crystallization of Amorphous Silicon Structures, 5(1), 35
- Illumination and Dark Current-Voltage Characteristics of Polymer-Silicon Heterojunction Solar Cells, L2(1), 12
- Influence of Deposition Parameters on Optical and Electrical Properties of Cu<sub>x</sub>S Thin Films Prepared Using Chemical Bath Deposition Method, 4(3), 19
- Investigation of Amorphous to Crystalline Transition in Glassy  $\text{Se}_{80}\text{Te}_{20}$  and  $\text{Se}_{70}\text{Te}_{20}\text{M}_{10}$  (M=Ag, Cd, Sb) Alloys, 1(3), 7
- Light-Beam-Induced-Current Analysis of Thin-Film Polycrystalline Solar Cells, 7(4), 29
- Modeling of Transport Properties of Amorphous Silicon Solar Cells, 6(1), 25
- Nano/Micro Surface Texturing and Enhancing of Photovoltaic Cells Efficiency by Using UV Femtosecond Laser Pulses, 7(2), 33
- Nickel Doping and Annealing Effects on the Structural and Optical Properties of Iron Oxide Thin Films, 10(3), 17
- Optical and Electrical Properties of Zinc Oxide Films Prepared by Spray Pyrolysis, 6(4), 23



- Optical and Electrical Properties of ZnO Thin Films Prepared by Spray Pyrolysis Technique, 4(1), 31
- Optical Properties of Annealed Cadmium Sulfide Thin Films Prepared by Chemical Bath Deposition, L2(2), 19
- Optical Properties of Many-Layers Zinc Sulphide Thin Films prepared by Chemical Bath Deposition Method, 6(3), 33
- Optical Properties of Thermally-Annealed Tin-Doped Indium Oxide Thin Films, L2(2), 15
- Optimization of Silicon Solar Cells Efficiency by Chemical Texturing, 10(2), 17
- Optoelectronic Characteristics of As-doped Silicon Photodetectors Produced by LID Technique, L1(2), 23
- Photocatalytic Performance of Mixed and Single Phases of Titanium Dioxide Nanoparticles on Growth of Fusarium Oxysporum Fungal, 17(4), 9
- Preparation and Characteristic Study of In<sub>2</sub>O<sub>3</sub>/c-Si Made by Spray Pyrolysis, 1(1), 11
- Preparation and Characterization of Self-Assembled n-ZnS Thin Films, 4(4), 33
- Preparation and Characterization of PAni Films by Electrochemical Polymerization, 10(2), 23
- Preparation and Study of Indium Oxide Nanoparticles, 10(4), 15
- Spectral and Electrical Characteristics of Nanostructured NiO/TiO<sub>2</sub> Heterojunction Fabricated by DC Reactive Magnetron Sputtering, 16(3), 39
- Stress Management and Interfacial Strength of Gallium Nitride Layer Grown on Diamond Substrate, 13(2), 19
- Structural Characteristics of Silicon Nitride Nanostructures Synthesized by DC Reactive Magnetron Sputtering, 15(4), 33
- Structural, Electronic and Gas Sensing Properties of Cu-Doped ZrO<sub>2</sub>-TiO<sub>2</sub>, 10(3), 23
- Structural Properties of Semiconducting Nanostructures Prepared by DC Plasma Reactive Sputtering Method, 10(3), 41
- Studying Defects on Semiconductor Surfaces by Photoacoustic Spectroscopy, 6(3), 25
- Synthesis of Silicon Nanowires by Selective Etching Process, 4(3), 15
- Technology and Future of III-V Multi-Junction Solar Cells, 6(3), 3
- The Effect of Some Experimental Parameters on the Properties of Porous Silicon, 4(1), 37
- Theoretical Treatment to Determine the Quality of Photonic Crystal Fiber (PCF) as a Function of the Number of Air Holes, 9(3), 31
- Thermal Management of Vertical External Cavity Surface Emitting Laser Grown on GaAs Substrate, 13(2), 15
- Thermally Stimulated Currents Technique to Study Traps in Insulators and Semiconductors, 11(2), 3
- Using Substrate Removal Technique for GaAs-Based VECSEL Optimization, 13(2), 23
- Analysis of Performance of ZnO/CdS/SnS Solar Cell Using Software Program SCAPS-1D 19(2), 9
- Comparative Study of Gamma and Beta Rays Exposure Effects on Manganese Sulphide Thin Films for Solar Cell Applications 19(1), 21
- Determining the Optimal Direction and Angle of Incidence of Solar Radiation to Obtain Electrical Energy from Solar Panels in the Nineveh Plain Area 19(3B), 20
- Fabrication and Improvement of Optoelectronic Properties of Copper Chalcogenide Thin Films 19(4C), 223
- Innovative Method to Prepare Highly Adhesive CuO Thin Films on FTO Substrates for Optoelectronic Applications 19(4A), 61
- Photoresponse and Quasi-two-dimensional Electron Gas Transport of Sm<sub>2</sub>O<sub>3</sub>/SrTiO<sub>3</sub> Heterointerfaces Films Prepared by Sol-gel Method 19(2), 43
- Preparation and Characterization of Copper Oxide Nanoparticles by Precipitation Method for Photonics and Optoelectronics 19(3A), 37
- Study the Effect of Molar Concentrations on the In<sub>2</sub>S<sub>3</sub>/Si Photodetector Performance 19(3B), 47
- Synthesis of NAC-CdTe/CdS Core-Shell Quantum Dots for Optical Biosensing Applications 19(1), 35
- Technical and Economic analysis criteria for optimal configurations in PV Battery Systems 19(4B), 83

### Solid State Physics & Applications

#### IJAP-SSPAA

- A Mathematical Model to Describe the Densification Process During the Sintering of Ceramic Compacts, 4(2), 11
- Antibacterial Activity of Gold and Silver Nanoparticles against Pathogen Species, *E. coli* and *S. aureus*, 13(3), 19
- Bulk Properties of YBa<sub>2</sub>Cu<sub>3</sub>O<sub>7</sub> Superconducting Materials, 1(2), 19
- Calculation of Buildup Factors for Ceramic Materials, 7(1), 23
- Characteristics of Gold and Silver Nanoparticles Deposited on Crystalline and Amorphous TiO<sub>2</sub> Films by Femtosecond Laser Pulses, 8(1), 43
- Characteristics of Indium Nitride Thin Films Deposited on Silicon Substrates by Reactive Sputtering with Nitride Buffer Layers, 18(2), 23
- Characterization of Commercial Al-Si Casting Alloys Reinforced with Nano SiC Composites, 8(3), 25
- Characterization of Epoxy Composites Reinforced by Waste Bio-Fibers, 11(3), 15
- Characterization of Indium Nitride Thin Films Prepared by Plasma-Assisted Molecular Beam Epitaxy, 18(3), 19
- Characterization of Multilayer Highly-Pure Metal Oxide Structures Prepared by DC Reactive Magnetron Sputtering Technique, 16(4), 25

- Characterization of Pulsed-Laser Deposited CuO-Doped MgO Thin Films for Gas Sensing Applications, 13(3), 13
- Characterization of SiC/SiC Composites Used for Power Plant Blanket, L2(1), 27
- Characterizations of Hydroxyapatite Thin Films Deposited by Spray Pyrolysis on Titanium Substrates for Bone Implant Applications, 10(3), 11
- Complex Magnetic Investigation of Ferritic Stainless Steel, L2(1), 9
- Comparative Study of Structural and Optical Properties of Silicon Dioxide Nanoparticles Prepared by DC Reactive Sputtering and Sol-Gel Route, 17(1), 17
- Conjunctional Freezing-Assisted Ultrasonic Extraction of Silicon Dioxide Nanopowders from Thin Films Prepared by Physical Vapor Deposition Technique, 15(4), 23
- Crystallization and Glass Transition Kinetics in  $\text{Se}_{90}\text{Sb}_{10-x}\text{Ag}_x$  Glassy Alloys, 9(1), 7
- Densification Behavior and Dielectric Properties of Low-Temperature Cordierite Ceramics, L1(2), 20
- Determination of Thermal Conductivity of Compact Graphite Iron, 4(4), 3
- Effect of Average Ionic Radius of A-site, B-site in  $\text{ABO}_3$  Perovskite Ceramics on Their Crystal Structures and Curie's Temperature, 17(2), 5
- Effect of Bio-Fiber Waste Addition on Specifications of Epoxy Composite, 11(1), 21
- Effect of Coir Fiber Length and Content on Mechanical Properties of Unsaturated Polyester Composites, 11(3), 27
- Effect of Gas Mixing Ratio on Energy Band Gap of Mixed-Phase Titanium Dioxide Nanostructures Prepared by Reactive Magnetron Sputtering Technique, 14(4), 19
- Effect of Operation Temperature on Characteristics of NiO-Doped Tellurium Oxide Thin Film Gas Sensors Prepared by Pulsed-Laser Deposition, 17(4), 3
- Effects of Annealing and Substrate Temperatures on Dielectric Properties of  $\text{CuInGaS}_2$  Structures Prepared by Quenching-Assisted Vacuum Coating Technique, 18(1), 9
- Effects of  $\text{CaO-B}_2\text{O}_3$  Glass on Sintering and Microwave Properties of Cordierite Ceramics for Low-Temperature Cofired, L1(1), 16
- Effects of Operation Parameters on Structures and Surface Morphology of Tin Dioxide Nanostructures Prepared by DC Reactive Sputtering, 16(3), 13
- Epitaxial and Structural Analysis of Nickel-Manganese-Gallium Films Prepared by Magnetron Sputtering, 14(4), 13
- Evaluation of Some Atomic Coefficients for Elements Carbon-Copper-Silver by Using Beta Particles, 10(1), 15
- Fabrication of Carbon Nanotube/Titanium Dioxide Nanocomposite Photocatalyst Using Sol-Gel Method, 12(2), 21
- Formation of Mid-Infrared Slot Antenna Arrays on Thin  $\text{Al}_2\text{O}_3/\text{Si}$  Structures Fabricated by Atomic Layer Deposition, 14(4), 25
- Highly-Pure Nanostructured Metal Oxide Multilayer Structure Prepared by DC Reactive Magnetron Sputtering Technique, 18(4), 9
- Influence of Complexing Agent on Morphology Properties of PbS Thin Films Studied by Atomic Force Microscopy, 11(2) 13
- Influence of Complexing Agents on Structural Properties of PbS Thin Films Prepared by CSD Method, 12(1), 23
- Influence of Functionalization MWCNTs Using Acid Treatment on Gram Negative and Gram Positive Bacteria, 10(3), 29
- Interfacial Adhesion of PZT Ferroelectric Thin Films Determined by Nano-Indentation Method (Rapid Communication), 5(1), 32
- Investigation of the Mechanical Behavior of Binary and Ternary Polymer Blends, 11(2), 19
- Key Mechanisms of Low-Pressure Glow Discharge in Magnetized Plasmas, 12(3), 3
- Key Principle of Electroluminescent Polymers (Review Article), 5(1), 3
- Low-Temperature Aqueous Chemical Growth of Inorganic-Organic Hybrid Junction with ZnO Nanorods/Polyfluorene Structure, 9(1), 29
- Microhardness of Nanostructured  $\text{Si}_x\text{N}_{1-x}$  Thin Films Prepared by Reactive Magnetron Sputtering, 12(2), 15
- Microstructural Study of Copper-Carbon Composite Interface, 6(2), 25
- Methods of Determining the Refractive Index of Thin Solid Films, 4(1), 17
- Micron-Scale Modifications of Silicon Surface Morphology by Pulsed-Laser Texturing, 16(2), 31
- Nanostructured CdSnSe Thin Films Prepared by DC Plasma Sputtering of Thermally Casted Targets, 14(4), 33
- Nanostructured Copper Oxide Thin Films Prepared by DC Reactive Magnetron Sputtering, 13(2), 11
- Polynanocrystalline  $\text{CuIn}_3\text{Se}_5$  Thin Film Photoabsorber Layer Produced by Pulsed-Laser Deposition, L3(1), 15
- Power Reduction in Flexible Silicon Thin Film Digital Circuits, 5(2), 19
- Preparation and Characterization of Eggshell Powder (ESP) and Study its Effect on Unsaturated Polyester Composites Material, 11(1), 25
- Preparation and Characterization of Ni-doped  $\text{TiO}_2$  Nanostructures for Surface Cleaning Applications, 17(1), 3
- Preparation and Characterization of Silicon Dioxide Nanostructures by DC Reactive Closed-Field Unbalanced Magnetron Sputtering, 12(4), 13
- Preparation and Characterization of Silicon Nitride Nanostructures Prepared by DC Reactive Sputtering Technique with Novel Design of Closed-Field Unbalanced Dual Magnetron Assembly, 13(3), 3

- Preparation and Structural Characterization of  $\text{Cu}_2\text{ZnSnS}_4$  Thin Films by Quenching-Assisted Coating Method, 17(4), 29
- Preparation of Highly Pure Nanostructures by Reactive DC Magnetron Sputtering Technique, 12(3), 27
- Preparation of Refractory Mortar from Iraqi Raw Materials, 11(2), 37
- Preparation of Zirconia Aerogel Nanostructures by Supercritical Drying Autoclave Method, 17(4), 23
- Production of Ceramic-Based Composites By Self Infiltration, 4(1), 25
- Scanning Tunneling Microscopy and Medium Energy Ion Scattering Spectrometry of Spinel Structure of  $\text{Li}_4\text{Ti}_5\text{O}_{12}$  Surface, 14(3), 21
- Structural Characteristics of Nickel Oxide-Doped Tellurium Oxide Thin Films Prepared by Pulsed-Laser Deposition, 17(3), 9
- Structural and Surface Characteristics of  $\text{Cd}_{0.9}\text{Sb}_{0.1}\text{Se}$  Thin Films Prepared by Thermal Evaporation, 14(1), 23
- Structural Characteristics of Nickel Ferrite Nanoparticles Synthesized by New Arrangement of Concentric Targets in DC Reactive Magnetron Sputtering, 12(4), 9
- Structural Properties of Nickel Oxide Nanostructures Prepared by Closed-Field Unbalanced Dual Magnetron Sputtering Technique, 13(2), 3
- Structural Characteristics of  $\gamma\text{-Al}_2\text{O}_3$  Nanoparticles Prepared by Laser-Assisted Spray Pyrolysis Technique, 11(2), 29
- Structural, Morphological and Photoluminescence Characteristics of  $\text{Cu}_2\text{S}$ -Doped Nanostructured ZnS Thin Films Deposited on Porous Silicon, 18(1), 31
- Temporally and Spatially Localized Phase Transformations in Ferrous Alloys for Materials Processing Applications, 17(1), 29
- Zinc Oxide Nanowires Prepared by Oblique Angle Deposition Method, 12(1), 3
- Characterization and Antibacterial Activity of Copper Oxide Nanoparticles Prepared Using Nd:YAG Pulsed-Laser Ablation 19(4B), 113
- Characterization and Antibacterial Activity of Titanium Dioxide Nanoparticles Prepared by Nd:YAG Pulsed-Laser Ablation 19(4C), 179
- Characterization of Electrochromism and Photoelectrochromism of N-Doped  $\text{TiO}_2$  and  $\text{Co}_3\text{O}_4$  Thin Films Prepared by DC Reactive Magnetron Sputtering: Comparative Study 19(1) 5
- Characterization of Poly Methyl Methacrylate (PMMA) Nanofiber Enhanced by the Chlorophyll 19(4C), 251
- Comparative Analytical Study of Some Stainless Steels Using LIBS, XRD, XRF and EDS Techniques 19(1), 41
- Comprehensive Investigation of Morphological, Structural, and Optical Properties of  $\text{NiO}:\text{Al}$  Films Prepared by Thermal Evaporation 19(4C), 217
- Determination of Mass and Linear Absorption Coefficient for Some reinforced polymeric materials from X-Ray Characteristics 19(3B), 30
- Effect of  $\text{Nb}_2\text{O}_5$  and  $\text{PdO}$  Coatings on Sensing Characteristics of Nanostructured  $\text{CdO}$  Thin Films 19(4A), 3
- Effect of Structural Phase on Photocatalytic Activity of Titanium Dioxide Nanoparticles 19(3A), 55
- Effect of Substrate and Annealing Temperature on Hall Effect and Activation Energy of  $\text{CuISe}_2$  Compound 19(3B), 43
- Enhanced Fatigue Characteristics of Aluminum Alloy 6082 Reinforced with  $\text{SiC}$  Nanoparticles 19(4C), 211
- Evaluation of Laser Influence on Optical Properties of Magnesium Oxide Thin Films Prepared by Drop Casting Method 19(2), 33
- Fabrication and Investigation of Structural, Optical and Dielectric Properties of  $\text{ZnO}:\text{MnO}_2$  Composites 19(4A), 21
- Initial Characterization of the Prepared Au-Decorated  $\text{TiO}_2$ :Fullerene Films Using Electrospray Method 19(4B), 151
- Investigation of Some Structural and Optical Properties of PMMA-PVA/PDA Nanocomposites 19(1), 29
- Mechanical Properties and Surface Morphology of Polyester Resin Supported by Titanium Oxide Nanoparticles 19(4A), 43
- Preparation and Characterization of Biomaterial Powder by Sol-gel Method 19(4A), 77
- Preparation and Characterization of Fullerene/ $\text{AuNPs}$  Composite Films 19(4B), 167
- Preparation and Characterization of Metal-Doped Titanium Dioxide Nanostructures by Sol-Gel Method 19(4A), 49
- Preparation and Wettability of Zinc Oxide Nanostructures by Oxidation of Zinc Foil in Hot Water 19(4A), 67
- Structural Characteristics of  $\text{TiO}_2/\text{TiN}$  Nanocomposites Synthesized by DC Reactive Magnetron Sputtering Technique 19(3A), 49
- Structural Properties of  $\text{CuPc}:(\text{Au}, \text{Ag})$  NPs Thin Films Deposited by Spin Coating Technique 19(3A), 19
- Structural, Morphological and Mechanical Characteristics of  $\text{Ni}_{55}\text{-Cu}_{45}$  Alloy Prepared by Powder Technology 19(4B), 157
- Structural, Optical and Electrical Properties of  $\text{TiO}_2:\text{MoS}_2$  Thin Films Prepared by Pulsed-Laser Deposition Technique 19(3A), 25
- Synthesis and Characterization of Ceramic System Beta Tri-calcium Phosphate Used in Teeth and Bones Substitutions 19(3A), 43
- Synthesis and Study the Structural and Optical Properties of  $\text{TiN}$  and  $\text{TiO}_2:\text{TiN}$  Nanostructures via DC Reactive Magnetron Sputtering Technique 19(4C), 229

- Thickness-Dependent Optical and Topographical Characteristics of Ferric Oxide Thin Films prepared by Spray Pyrolysis 19(4B), 145

\* \* \*

**Notes:**

- 1(1), 3 refer to IJAP, Vol. 1, No. 1, page 3
- L1(1), 3 refer to IJAPLett, Vol. 1, No. 1, page 3